Empirical derivation of the reference region for computing diagnostic sensitive 18fluorodeoxyglucose ratios in Alzheimer's disease based on the ADNI sample[☆,☆☆]

Jerod M. Rasmussen [a,*], Anita Lakatos [a], Theo G.M. van Erp [a], Frithjof Kruggel [b], David B. Keator [a], James T. Fallon [a], Fabio Macciardi [a], Steven G. Potkin [a]
for the Alzheimer's Disease Neuroimaging Initiative

[a] Department of Psychiatry and Human Behavior, University of California Irvine, Irvine, CA, USA
[b] Department of Biomedical Engineering, University of California Irvine, Irvine, CA, USA

ARTICLE INFO

ABSTRACT

Careful selection of the reference region for non-quantitative positron emission tomography (PET) analyses is critically important for Region of Interest (ROI) data analyses. We introduce an empirical method of deriving the most suitable reference region for computing neurodegeneration sensitive 18fluorodeoxyglucose (FDG) PET ratios based on the dataset collected by the Alzheimer's Disease Neuroimaging Initiative (ADNI) study. Candidate reference regions are selected based on a heat map of the difference in coefficients of variation (COVs) of FDG ratios over time for each of the Automatic Anatomical Labeling (AAL) atlas regions normalized by all other AAL regions. Visual inspection of the heat map suggests that the portion of the cerebellum and vermis superior to the horizontal fissure is the most sensitive reference region. Analyses of FDG ratio data show increases in significance on the order of ten-fold when using the superior portion of the cerebellum as compared with the traditionally used full cerebellum. The approach to reference region selection in this paper can be generalized to other radiopharmaceuticals and radioligands as well as to other disorders where brain changes over time are hypothesized and longitudinal data is available. Based on the empirical evidence presented in this study, we demonstrate the usefulness of the COV heat map method and conclude that intensity normalization based on the superior portion of the cerebellum may be most sensitive to measuring change when performing longitudinal analyses of FDG-PET ratios as well as group comparisons in Alzheimer's disease. This article is part of a Special Issue entitled: Imaging Brain Aging and Neurodegenerative disease.

© 2011 Published by Elsevier B.V.

1. Introduction

Careful selection of the reference region for computing radiopharmaceutical and radioligand ratios in non-quantitative positron emission tomography (PET) studies is critically important, in particular for diseases that may differentially affect brain regions, such as Alzheimer's disease (AD). While several studies have shown that data-driven selection of a normalization region for PET ratio group comparison studies is superior to global mean normalization [1–4], no study to date has empirically derived the optimal denominator region for computing *degeneration sensitive 18fluorodeoxyglucose (FDG) ratios*. The longitudinal design of the Alzheimer's Disease Neuroimaging Initiative (ADNI) study is uniquely suited to this data analysis.

Absolute values of cerebral metabolic rates of glucose (CMRgl) as measured by FDG-PET in the ADNI sample show large amounts of intra- and inter-subject and site (scanner) variability that limit data analyses. This unwanted variance is significantly reduced by averaging over multiple acquisitions and by computing FDG ratios based on reference regions [5]. Averaging increases the signal to noise ratio and computation of ratios to a reference region cancels out unwanted intra- and inter-subject and site variability, thereby facilitating greater ability to significantly detect smaller group differences. It is critically important to choose a reference region that robustly removes the unwanted variance but not the effects of the disease and/or its progression. This may be particularly challenging for neurodegenerative disorders that differentially affect much of the brain.

A selective review of the PET FDG literature on Alzheimer's disease and aging shows the use of a wide variety of normalization regions, including the whole brain [6–9], the cortex [10], the calcarine cortex

and basal ganglia [11], the cerebellum [7], the pons [1,12–14], and the combined cerebellum, vermis and pons [15]. The use of different normalization regions may contribute to inconsistent and spurious findings across studies. Borghammer and colleagues [16,17] have shown that an undetected decrease in normalization regions, e.g., mean whole brain FDG, can result in the creation of artificial hypermetabolism in unaffected regions and spurious relationships between FDG ratios and demographic or other clinical variables.

Given the importance of normalization region selection and available longitudinal data, we set out to empirically derive the most suitable normalization region for longitudinal studies in Alzheimer's disease. We employ the use of visual inspection of a heat map depicting differences in coefficients of variation across time among all Automated Anatomical Labeling (AAL) atlas regions, normalized by all other AAL atlas regions, as well as the criterion of the largest change over time. The most suitable ratios computed should show the largest amount of change over time in regions known to be affected by Alzheimer's disease. To our knowledge, this is the first PET study to empirically derive the optimal denominator region for computing degeneration sensitive ^{18}fluorodeoxyglucose ratios longitudinally in Alzheimer's disease.

We first examined differences in annualized percent change in absolute and un-normalized FDG uptake between healthy elderly and Alzheimer's disease patients in order to get an initial estimation of regions that may show change in FDG uptake over time. Subsequently, we derived candidate normalization regions based on an Alzheimer's disease versus healthy elderly control coefficient of variation difference in the heat map. We predicted that normalization using the optimal denominator region would show the largest change in FDG PET ratios over time compared with normalization based on other candidate regions or whole brain FDG. Additionally, we explored whether regions that show the largest mean annualized percent degeneration in Alzheimer's disease also show the largest group differences between AD patients and healthy elderly volunteers. Given that AD is a progressive neurodegenerative disorder, we predicted a positive association between mean annualized percent change in FDG PET ratio in Alzheimer's disease and mean group differences between AD patients and healthy elderly volunteers. Finally, we hypothesized that the FDG ratios that are the most sensitive to degeneration also show the strongest group differences when comparing AD patients with healthy elderly volunteers.

2. Materials and methods

2.1. Ethics

The ADNI study was approved by each of the participating sites' Institutional Review Boards (IRBs) and complied with the Code of Ethics of the World Medical Association (Declaration of Helsinki). Written informed consent was obtained from all participants after they had received a complete description of the study.

2.2. The Alzheimer's Disease Neuroimaging Initiative (ADNI)

ADNI was launched in 2003 by the National Institute on Aging (NIA), the National Institute of Biomedical Imaging and Bioengineering (NIBIB), the Food and Drug Administration (FDA), private pharmaceutical companies, and non-profit organizations as a $60 million, 5-year public–private partnership. The primary goal of ADNI is to test whether serial magnetic resonance imaging (MRI), positron emission tomography (PET), other biological markers, such as cerebrospinal fluid (CSF) markers, APOE status and full-genome genotyping via blood sample, and clinical and neuropsychological assessments can be combined to measure the progression of mild cognitive impairment (MCI) and AD. Determination of sensitive and specific markers of very early AD progression is intended to: (1) aid in the development of new treatments, (2) increase the ability to monitor their effectiveness, and (3) reduce the time and cost of clinical trials.

The principal investigator of the initiative is Michael W. Weiner, M.D., of the Veteran's Affairs Medical Center and University of California, San Francisco. ADNI is the result of efforts of many co-investigators from a broad range of academic institutions and private corporations, and participants have been recruited from over 50 sites across the U.S. and Canada. ADNI participants range in age from 55 to 90 years and include approximately 200 cognitively normal elderly followed for 3 years, 400 elderly with MCI followed for 3 years, and 200 elderly with early AD followed for 2 years. Participants are evaluated at baseline, 6, 12, 18 (for MCI only), 24, and 36 months (AD participants do not have a 36 month evaluation). Baseline and longitudinal follow-up structural MRI scans are collected on the full sample and 11C-labeled Pittsburgh Compound-B (11C-PIB) and ^{18}FDG PET scans are collected on a subset every 6–12 months (for study details see http://www.adni-info.org) [18].

2.3. Study samples

In this study, data analyses were conducted on two sub-samples derived from the complete ADNI sample. Both sub-samples were confined to individuals with mild probable Alzheimer's disease (AD) and healthy control (HC) samples as determined at the baseline assessment. The first sample comprised 117 individuals (60 AD and 57 HC) with baseline, 6, 12 and 24-month follow-up ^{18}FDG PET assessments. The second larger sample comprised 199 individuals (97 AD and 102 HC) who had baseline ^{18}FDG PET assessments. General eligibility criteria for participation in the ADNI study include age between 55 and 90 years, English or Spanish speaking, as well as the willingness and ability to undergo all test procedures including neuroimaging and longitudinal follow up assessments. Participants were assessed with the Mini Mental State Examination (MMSE) [19], the Clinical Dementia Rating sum-of-boxes (CDR-sob) [20], and the Alzheimer's Disease Assessment Scale-cognitive subscale (ADAScog) [21]. Diagnoses of AD were based on NINCDS/ADRDA criteria [22] including MMSE scores between 20 and 26 and CDR scores 0.5 or 1.0. Healthy controls have MMSE scores between 24 and 30 and a CDR of 0, are non-depressed, non-MCI, and non-demented (for details see: http://www.adni-info.org/Scientists/ADNIGrant/ProtocolSummary.aspx).

Comparisons of demographic data showed lower ADAS-cog scores, lower MMSE scores, higher CDR global values, similar mean age, similar mean socioeconomic status, similar smoking history, as well as similar sex and handedness distributions in the AD compared with the HC groups in both study samples. However, the AD groups had a lower education level and disproportionately higher APOE4 allele frequencies compared with the HC groups (Table 1).

Table 1
Sample 1 and sample 2 demographics.

	Sample 1				Sample 2			
	HC (n = 60)	pAD (n = 57)	Statistic	p-value	HC (n = 102)	pAD (n-97)	Statistic	p-value
Demographic								
Mean age	75.4 ± 4.6	76.0 ± 6.5	$t_{115} = 0.57$	0.57	75.93 ± 4.8	75.68 ± 7.32	$t_{197} = 0.28$	0.77
Sex (male/female)	39/21	33/24	$\chi^2_1 = 0.62$	0.43	62/40	58/39	$\chi^2_1 = 0.02$	0.89
Smoker/non-smoker	23/37	13/44	$\chi^2_1 = 3.3$	0.07	39/63	33/64	$\chi^2_1 = 0.38$	0.54
Handedness (right/left)	53/7	57/0	FET	0.01**	92/10	92/5	FET	0.21
Ethnicity								
Hispanic/non-Hispanic/unknown	0/59/1	0/56/1	FET	1.0	1/99/2	1/94/2	FET	0.99
Race								
African-American/Asian/White	4/1/55	3/1/53	FET	1.0	8/1/93	5/2/90	FET	0.61
Mean years of education	16.2 ± 2.97	14.5 ± 3.	$t_{115} = 2.91$	0.0043**	15.85 ± 3.1	14.64 ± 3.21	$t_{196} = 2.66$	0.0083**
MMSE	29 ± 0.9	24 ± 2.0	$t_{78} = 19.05$	0.0001**	28.9 ± 1.1	23.47 ± 2.14	$t_{143} = 22.41$	0.0001**
ADAS-cog	6.8 ± 3.0	18.4 ± 6.1	$t_{80} = 12.85$	0.0001**	6.82 ± 2.91	19.11 ± 6.52	$t_{131} = 16.8$	0.0001**
APOE (ε2/ε3/ε4)	10/90/20	5/58/51	$\chi^2_2 = 21.98$	0.0001**	23/153/28	7/108/79	$\chi^2_1 = 40.37$	0.0001**
CDGlobal (0-0.5-1)	60-0-0	0-23-34	FET	0.0001**	60-0-0	0-23-34	FET	0.0001**
Scan resolution (low/high)	53/7	46/11	$\chi^2_1 = 1.3$	0.25	81/21	76/21	$\chi^2_1 = 0.034$	0.85

Mean ± standard deviation (SD) and the frequency of each category are represented with test statistics. ** Denotes significance at p<.005.
FET = Fisher's Exact Test (2-tailed).

2.4. Image acquisition and preprocessing

High-resolution structural MRI and two pre-processed sets of ^{18}FDG PET baseline, 6, 12, and 24-month follow-up assessment brain scans were obtained from the ADNI database (http://www.loni.ucla.edu/ADNI). The structural scans were unprocessed straight sagittal 3D MPRAGE acquisitions with a resolution close to 1 mm isotropic, collected on 1.5T General Electric, Philips, or Siemens scanners at more than 50 data collection sites (http://adni.loni.ucla.edu/research/protocols/mri-protocols). The ^{18}FDG pet datasets included absolute and intensity normalized scans. The absolute scans were co-registered and averaged by ADNI, while intensity normalized scans were also standardized with regard to image resolution, voxel size, and smoothness. The procedures are detailed on the ADNI website (see points 2 and 4 of the "Processed PET image data" section at http://adni.loni.ucla.edu/about-data-samples/image-data/). Briefly, all raw PET images were converted to a standard file format. Six five-minute frames 30–60 minute post ^{18}FDG-injection were extracted from the image file. The extracted frames were registered to the first frame (acquired at 30–35 min post-injection) and averaged to yield a single 30-minute average PET image in "native" space with a resolution of $128 \times 128 \times 63$ voxels and a 2 mm isotropic resolution. The average image of the baseline scan was reoriented such that the anterior–posterior axis of the image grid is parallel to the AC-PC line and the image was re-sampled to a resolution of $160 \times 160 \times 96$ voxels with a 1.5 mm isotropic resolution. All individual frames from each PET scan, baseline and follow-up, were then co-registered to this reoriented baseline reference scan and an average image for each assessment point was created. Each average image was intensity normalized using a subject-specific mask, in that the average intensity of voxels within the mask becomes exactly one. Each voxel intensity value is therefore an FDG/mean (of whole brain) ratio. Datasets were smoothed to a uniform isotropic resolution of 8 mm full width half maximum, the approximate resolution of the lowest resolution scanners used in ADNI. The specific filter settings were determined from the Hoffman phantom PET scans that were acquired during the ADNI certification process. Prior to image analysis all structural and PET scans were converted from DICOM to Brain Image Analysis (BRIAN) format.

2.5. Extraction of mean FDG for AAL atlas ROIs

To compensate for structural differences between diagnoses during registration, separate anatomical group atlas templates were generated for the AD patients and healthy elderly controls. Briefly, baseline T1-weighted MRI scans were aligned with the stereotaxic coordinate system [23]. A quality check was performed on the successful conversion and registration. The outer hulls of the brain were removed by a registration approach [24], yielding the "peeled" brain in the intracranial space (IC). Subsequently, all brain datasets were registered with the MNI 152 brain using a recent approach for nonlinear registration based on fluid dynamics [25]. All registered brains were averaged, correcting for their mean whole brain intensity, to yield the ADNI template 1. All brain datasets were registered to the ADNI template 1, and averaged voxelwise to yield the ADNI template 2. All brain datasets were registered with their group specific ADNI template 2, resulting in a deformation field for each subject. Preprocessed PET data were registered with the baseline "peeled" MRI brain using rigid body registration and normalized mutual information as similarity criterion. The deformation fields were used to warp the ^{18}FDG PET data into MNI space. The ADNI template 2 in MNI space was divided into ROIs using the AAL atlas [26] and absolute as well as whole-brain normalized FDG means for each of the AAL template ROIs were computed.

2.6. Longitudinal analysis of absolute FDG data

To determine whether glucose metabolism in the various reference regions changed over time between comparison groups, we performed a longitudinal analysis on the absolute ^{18}FDG PET ROI data. Absolute data was examined to take advantage of the unique repeated measures design of the ADNI PET sample while uncoupling the measurements from the whole brain normalization step that uses a scale factor not publicly available from ADNI. Given that the absolute data is not normalized by any region (whole brain or otherwise) and therefore has a high degree of variability, we computed the annualized percent signal change during the two year follow-up period based on the three available follow up assessments Eq. (1). As a ratio, this metric removes site and subject variance and averages visit-related noise effects. The annualized percent signal change (δ) was computed using the mean signal (S) in each subject (N) and ROI (j).

Eq. (1). Annualized Percent Signal Change in Absolute ^{18}FDG by Subject and ROI.

$$\delta_{N,j=116} = \frac{1}{3}\left[\frac{4(S_{6(N,j)} - S_{0(N,j)})}{(S_{6(N,j)} + S_{0(N,j)})} + \frac{4(S_{12(N,j)} - S_{6(N,j)})}{(S_{12(N,j)} + S_{6(N,j)})} + \frac{2(S_{24(N,j)} - S_{12(N,j)})}{(S_{24(N,j)} + S_{12(N,j)})} \right] \tag{1}$$

Group means and standard errors for AD patients and healthy elderly controls were calculated for every ROI. To remove extreme outliers, the data was systematically trimmed prior to the annualized percent change calculation. The optimal trim threshold was set at 10% of the time point *absolute* differences in each group to prevent rejection of true effect related outliers and was robust within 3% of this threshold. A larger threshold rejected true effects and drove the baseline up, while a lower threshold included extreme outliers and introduced instability in the baseline value. All trimmed outliers reflected nonsensical changes greater than 100% annually.

2.7. Empirical derivation of FDG ratio denominator region

To identify the reference region(s) that will result in ^{18}FDG ratios that are most sensitive to small changes in metabolism in key brain regions known to be affected by Alzheimer's disease, we computed coefficients of variation (COVs) for each of the 116 ROIs normalized by all of the 116 ROIs. COVs are capable of capturing linear and non-linear dispersion of FDG ratios over time. Only ROI data derived from the intensity-normalized ^{18}FDG PET data were used for the computations. The approach taken is formalized in the following paragraphs.

First, we created a matrix A_{ij}, comprised of 116 unique FDG ratios of one ROI to another for each of the 116 AAL atlas ROIs. This matrix comprises 116 rows by 116 columns and was created for each subject and time point in the sample data set.

Eq. (2). Ratio matrix definition.

$$A_{i,j=116} = \frac{A_i}{A_j} \tag{2}$$

Second, we concatenated the 2-dimensional matrix A over time (baseline, 6, 12, and 24 months) resulting in a 3-dimensional matrix for each subject with 116 rows by 116 columns by four time points. The COV, $c_{i,j}$, in each element of the matrix was defined by collapsing across time using Eq. (3), where µ and σ are the mean and standard deviation across time, respectively.

Eq. (3). COV.

$$c_{i,j} = \frac{\sigma_{i,j}}{\mu_{i,j}} \tag{3}$$

Third, we concatenated matrix c across subjects into the resulting matrix C with 116 rows by 116 columns by $N_{subjects,}$ where each cell contains a COV. This matrix is collapsed once more across AD patients and healthy elderly controls by taking the mean for each group. This results in the two final heat maps, one for each group, with 116 rows and 116 columns containing the mean COVs for each of the AAL regions normalized by all other AAL regions. The matrix <COV> is the mean normalized dispersion over time across subjects for a diagnostic group. This measure reflects the generalized dynamic nature of a given ROI ratio over time.

Eq. (4). <COV>, heat map.

$$<COV_{i,j}> = \frac{\sum_{k=1:N} C_{i,j,k}}{N} \tag{4}$$

Finally, to assess the differences in temporal dynamics between the groups, AD and HC were contrasted through a simple subtraction $<COV_\Delta> = <COV_{AD}> - <COV_{HC}>$.

2.8. Longitudinal analysis of FDG ratios based on candidate reference regions

Based on the empirical results of COV and longitudinal analysis of absolute FDG data, candidate reference regions were identified and examined for their respective sensitivities to relative metabolic change in the AD and HC samples. Using whole brain as a reference region, percent change relative to baseline was calculated for each subject and time point in a region traditionally considered to be stable across time (bilateral basal ganglia *sans* caudate) as well as a region typically implicated in AD (bilateral posterior cingulate). Each time point was averaged across subjects, keeping diagnosis separate. This calculation was repeated in three reference regions in addition to whole brain that were chosen to best reflect reference regions popular in current literature while carrying forward the results of the COV heat map: basal ganglia without caudate, entire cerebellum, and bilateral superior cerebellum including vermis. The superior cerebellum ROI referenced here and throughout this work is defined by those areas superior to the horizontal fissure and include AAL atlas regions: cerebellum III, IV, V, VI as well as the entire vermis.

2.9. Association between annualized percent change and group difference

Longitudinal changes in CMRgl and cross-sectional group differences in CMRgl were examined to assess the inferences they may have on one another. Group difference was defined and calculated as the percent difference between AD and HC relative to HC in all AAL regions, normalized by bilateral superior cerebellum and vermis. The normalization region was chosen to reflect the region identified by the COV heat map analysis. This was done for every time point and averaged in each ROI. Annualized percent change was defined relative to baseline and was calculated

with the same reference region as the group difference metric. These were then plotted against each other and correlated to yield a Pearson's correlation coefficient, r.

2.10. Statistical analyses

In the longitudinal analysis of absolute [18]FDG data, two sample t-tests were performed for every ROI to determine differential changes in [18]FDG uptake over time between AD patients and healthy elderly controls. In the COV analysis, candidate denominator reference regions were selected based on regions showing the largest difference in COV by visual inspection of the AD minus HC COV subtraction heat map (Fig. 6). In addition, the prevalence of denominator regions used in the established Alzheimer's disease PET literature as well as evidence of no differential change over time based on the longitudinal analysis of absolute FDG uptake were taken into account. Where multiple AAL ROIs were combined to form the denominator region, weighted means based on ROI intensities and ROI volumes were computed.

To identify the reference region that resulted in the best separation of AD patients and healthy elderly controls, univariate ANCOVAs predicting FDG ratios for each selected reference region (whole brain, basal ganglia, cerebellum, cerebellar vermis) with diagnosis (AD, HC), covarying for age, sex, and race, were performed. Group contrasts (t-tests) were performed to assess which regions showed significantly different FDG ratios between AD and HC. A Bonferroni correction based p-value (<0.0004) was used to control for multiple comparisons (116 ROIs). The AAL atlas regions showing significant group contrast for each of the reference regions are presented on a standard brain (Fig. 6).

3. Results

3.1. Longitudinal analysis of absolute [18]FDG data

The longitudinal analysis showed that FDG uptake in superior cerebellum regions did not decrease in either AD patients or healthy elderly controls during the two-year follow-up period (Fig. 1 top, middle). The comparison of annualized absolute percent signal change between healthy controls and patients showed non-significant global declines in whole brain FDG update in AD patients (3.3%) and healthy elderly controls (0.3%). Group contrasts showed several cerebral ROIs that had significantly larger rates of decline in AD patients compared with controls (Fig. 1 bottom). However, none of these differences survived Bonferroni correction for multiple comparisons. AD patients did show significantly larger decreases in FDG uptake in the supratentorial (3.5%) when compared with the infratentorial (1.6%) region (p<0.0001). Comparable rates in controls were 0.38% vs. 0.15%. There was some regional variation in the level of decline among the supratentorial regions, with the basal ganglia *sans* caudate at 2.4%, the parietal lobe at 3.1%, the occipital lobe at

3.3%, the frontal lobe at 3.3%, the limbic areas at 4.1%, and the temporal lobes at 4.4% decrease in glucose metabolism per year.

3.2. Coefficient of variation analysis

Visual inspections of the group COV heat maps show a clear global COV increase in AD when compared to HC (Fig. 2). Despite the global difference, there are a number of similar features between the two maps. Notably, the map bound by the cerebellum regions vertically and other regions horizontally (AD .044+/−.007, CTRL .036+/−.006) as well as the limbic regions vertically and other regions horizontally (AD .045+/−.008, CTRL .038+/−.006) show increased COV relative to the rest of the map (AD .036+/−.009, CTRL .029+/−.007). Two regions in both groups stand out (the bilateral mid-orbital frontal and bilateral cerebellum 10 AAL regions) as showing especially large variability over time. Intralobe pixels, those regions found slightly off diagonal that have high spatial correlation, are expectedly smaller than interlobe pixels, those regions that are found well off diagonal with low spatial correlation. An exception to this observation can be seen within a subsection of the infratentorial region (bilateral cerebellum
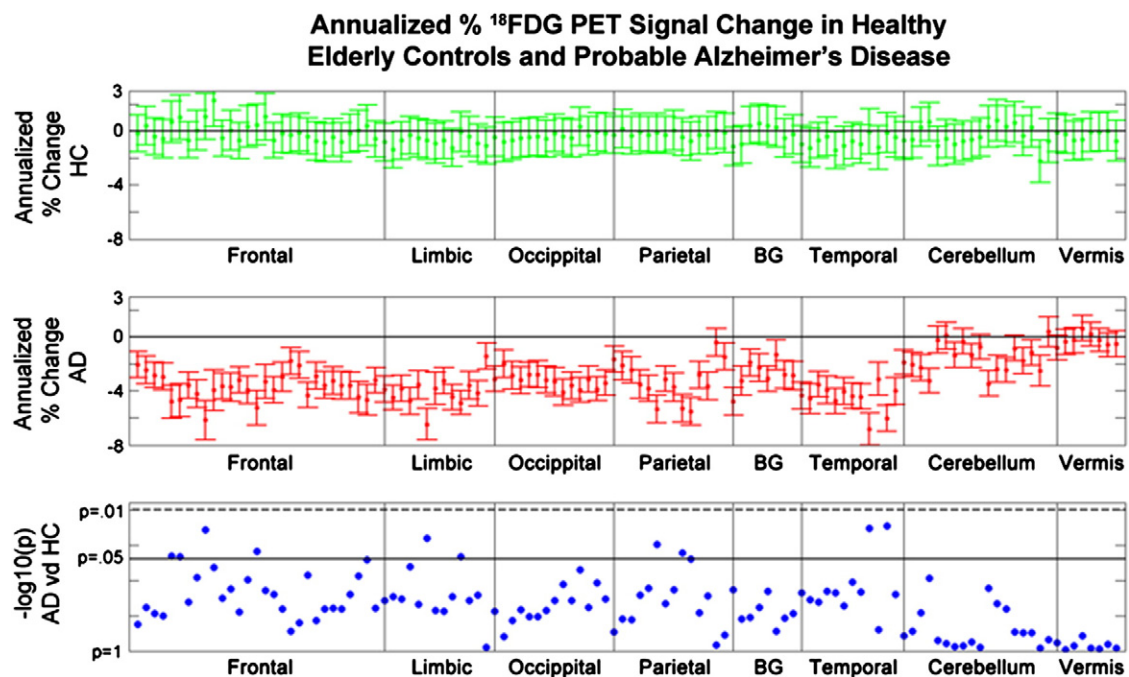

Fig. 1. Annualized percent change (+/− standard error) in un-normalized CMRgl between baseline, six, twelve and twenty-four-month follow-up across all AAL atlas regions of interest. Top row: Healthy Controls (HC), middle row: probable Alzheimer's disease (AD), bottom row: significance difference between groups. Each dot represents a single ROI defined in the AAL atlas.
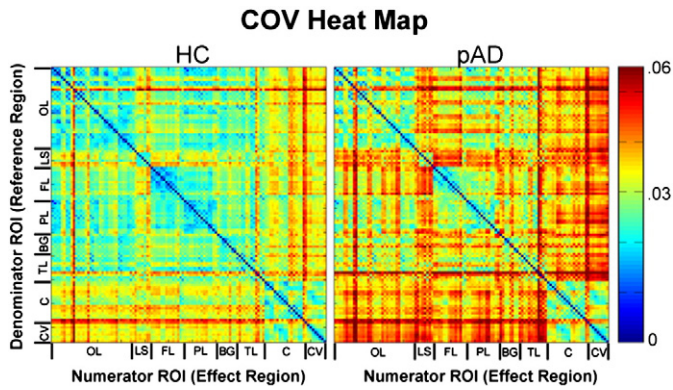
Fig. 2. COV heat maps of NC and AD groups. Hotter pixels reflect greater relative time variability, indicative of increased sensitivity to metabolic change differences in the AD population. Map similarities include COV hyperintensities in cerebellum and limbic regions. Cooler regions indicate spatial correlation (those regions near to the diagonal) and/or temporal correlation (those regions well off diagonal). Temporal correlation suggests coherence in rate of CMRgl change over time. CV: cerebellar vermis, C: cerebellum, TL: temporal lobe, BG: basal ganglia, PL: parietal lobe, OL: occipital lobe, LS: limbic system, and FL: frontal lobe.

10). Cooler regions well off the diagonal are reflective of low variability relative to the mean, due to temporal CMRgl correlation between the numerator and denominator that is independent of spatial correlation.

Visual inspection of the (AD–HC) COV contrast map addresses the primary aim of the COV analysis: to differentiate, between groups, which normalizing regions are the most reflective of both linear and non-linear regional changes over time. Hotter features reflect increased CMRgl temporal dynamics in AD compared to HC. Because each pixel's temperature is a reflection of one region normalized by another, the map is symmetric. As an example of this, it is clear that the temporal lobe has a higher COV whether it is the numerator or the denominator, demonstrated by the hot bars in the temporal lobe both vertically (temporal as the denominator) and horizontally (temporal as the numerator). AD subjects have larger COV values across 95% of all brain regions, a testament to the degenerative nature of the disease. Those regions that are preferentially targeted by the disease show larger COV increases from HC to AD, in particular temporal lobe, parietal lobe and the limbic system. Specific features motivate the selection of reference regions in Section 2.8. Candidate reference regions are composed of several hot regions with the
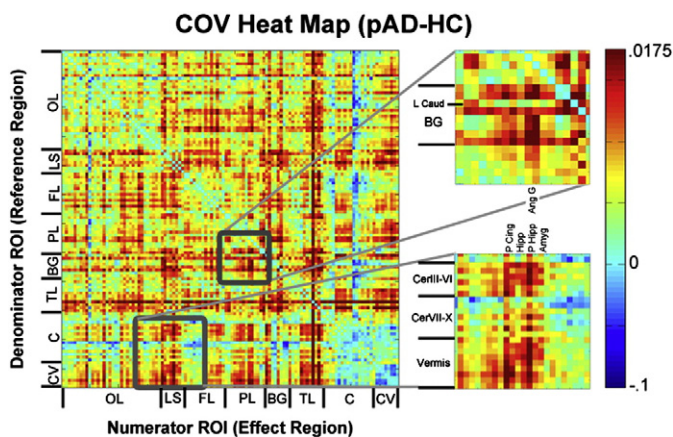

Fig. 3. Coefficient of Variance (COV) heat map, AD–NC. Each pixel represents an effect size ROI normalized by a reference ROI. Note decreased COV in AAL Cerebellum 1–2 and 7–10 relative to the rest of the cerebellum, as well as the smaller COV present in the caudate region of basal ganglia. Both of these observations are motivating factors for the modified reference regions used in the statistical analysis portion of the manuscript.

exclusion of cool regions within the area (jump out boxes in Fig. 3). Hot regions include the basal ganglia (excluding caudate which is cool), a subset of cerebellum including regions III, IV, V and VI with the entirety of the vermis, the full cerebellum and the whole brain.

3.3. Longitudinal analysis of FDG ratios based on candidate normalization regions

Analysis of percent change over time in two ROIs, one implicated in disease and one thought to be spared by the disease, showed marked differences between the perceived rate of change in CMRgl based on the reference region used to compute the ratios. The posterior cingulate was identified by all four reference regions to be significantly different from AD at the 24-month visit. However, only full and partial cerebellum reference ROIs were able to wean out this effect by the one year point and only by using the partial cerebellum as the denominator region were we able to show group differences at the earliest follow up visit, 6 months. In addition to being the most significant, partial cerebellum proved to be the most sensitive to relative CMRgl changes, having an average decline of 8.7% in 2 years for bilateral posterior cingulate ROIs. The average control subject declined in CMRgl at all three follow-up time points relative to all reference regions, with a maximum of no more than 1.4% per year. Examining a stable region yielded dramatically different results. Redundantly, basal ganglia as the reference region showed no change over time, essentially a null result as this region should roughly normalize to unity at all time points. Provocatively, basal ganglia regions were shown to be significantly decreased relative to full and partial cerebellum at 12 and 24 months respectively. CMRgl decline was as great as 2.8% over 2 years using partial cerebellum as the denominator. Whole brain normalization, on the other hand, suggested neurodegeneration in the basal ganglia to be non-existent in AD (Fig. 4). On the contrary it was shown to significantly *increase* by the two year mark by 2.7%.

3.4. Association between annualized percent change and mean effect size

In order to make inferences about AD from longitudinal changes in CMRgl it is important to know the relationship between it and cross-sectional group differences. Annualized percent changes relative to partial cerebellum in all ROIs were in the range of −4.8% to +1.0%. The measured group difference, relative to HC, had a range of −19.2% to +1.8%, reflecting the cumulative toll of the disease on neurodegeneration. Plotting and correlating these two metrics (Fig. 5) showed a significantly strong correlation between the two (r = .84). There is suggestion of an asymptote at the 0% mark, populated mostly by those ROIs involved in normalization.

3.5. GLM analysis of group differences

As a final metric for comparison of reference regions, t-tests of the ANCOVA model beta values were performed to highlight similarities and differences in identifying significant group differences between the regions used in normalization (Fig. 6). Using the whole brain as a reference region, as done in previously published ADNI studies, large portions of the cerebellum and basal ganglia were uniquely identified as being affected by the disease. The regions deemed significant no matter the choice of reference regions, were limited to part of the temporal lobe, angular gyri, hippocampus and posterior cingulate. The reference region identified in this analysis that revealed the largest ROI group differences was the superior cerebellum and vermis. In addition to identifying all regions identified by basal ganglia and the full infratentorial ROI, this specific reference ROI identified multiple regions of the frontal lobe, as well as the R mid temporal pole, R anterior cingulate, and superior parietal and occipital lobes. Overall, 94 of the 116 regions were identified as affected by AD with one of the
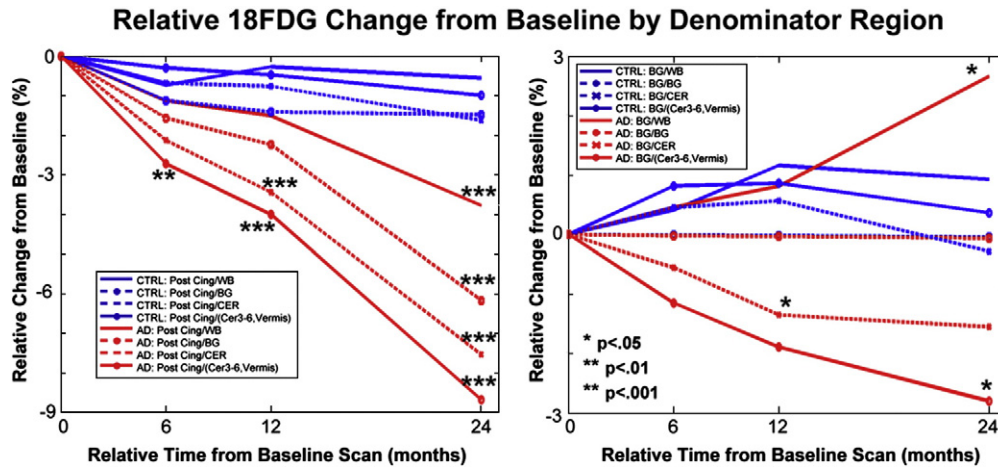
Relative 18FDG Change from Baseline by Denominator Region

Fig. 4. Longitudinal example of relative neurodegeneration by denominator region, the ROI on the left (LR combined posterior cingulate) is traditionally associated with AD, while the ROI on the right (LR combined pallidum, putamen and thalamus) is traditionally thought to be spared by the disease. HC and AD represent blue and red lines respectively. Combined cerebellum III, IV, V, VI and vermis as a reference region was shown to be the most sensitive to neurodegeneration, while whole brain normalization significantly identified the basal ganglia regions to be increasing with disease progression.

above reference regions. As the most sensitive region for differentiating groups was the superior cerebellum which accounted for 68% of the 94 regions. This is in contrast to 54%, 33% and 44% for infratentorial, basal ganglia, and whole brain respectively. In addition to the increased spatial extent of group differences, ROIs typically implicated in the disease show large increases in significance when using the superior portion of the cerebellum relative to the cerebellum in full. For example, L posterior cingulate and L hippocampus showed 20- and 50-fold gains in significance respectively.

4. Discussion

In the attempt to empirically derive the optimal reference region for detecting neurodegenerative metabolic decline in Alzheimer's disease, five principal findings emerged: 1) while large extents of the cerebrum and inferior cerebellum do decrease in CMRgl over time in AD, the superior cerebellum including vermis does not, 2) FDG ratios normalized by superior cerebellum and basal ganglia regions have the highest COVs in Alzheimer's disease patients when compared to healthy elderly volunteers, 3) among the candidate normalization regions, FDG ratios normalized with the superior cerebellum show the steepest rate of decline over time when compared with whole brain, basal ganglia and full cerebellum reference regions 4) mean

Annualized Percent Change As A Predictor of Effect Size

Fig. 5. Mean effect size as measured by the difference between normalized HC and AD, averaged across all four time points, plotted against annualized ¹⁸FDG percent change for all 116 AAL ROIs. A strong correlation between the cross-sectional effect size and longitudinal rate of neurodegeneration is seen.

annualized percent signal change in AD patients is strongly correlated with mean cross-sectional AD-HC group differences and 5) among all candidate reference regions, superior cerebellum is the most sensitive in identifying AD–HC group differences.

In order to express regional changes over time independent of all other regions it is imperative to use absolute, non-normalized data. ADNI's preprocessing pipeline includes measures to account for differences in site, subject and visit. This includes whole-brain normalization, a preprocessing step that renders data no longer independent of other voxels. Because of this, absolute unprocessed data is needed if one chooses to make statements regarding absolute changes over time free of influence from other voxels. In addition to site differences, the unprocessed data is susceptible to physiological and visit differences within subject. Variation in FDG PET determined CMRgl has been shown to be tightly coupled to CBF [27], making it a relevant factor in examining day to day variations in PET quantification. Subject variation in CBF is a function of both age and sex, among other factors, and can have a normal CBF range of 43–69 (ml/100 g/min) when measured by Arterial Spin Labeling (ASL) [26]. Visit differences are a function of, among other things, day-to-day variation in CBF. These fluctuations have been shown to be roughly 9% between one-week session intervals in ASL [28,29]. Using a percent absolute signal change within subject, across time, one can divide out both the site and subject level variances. However, visit level variance will still be present.

Systematic trimming played a deterministic role in the baseline value of absolute annualized percent change. As a numerical example without trimming, HC subjects were observed to have a greater than 3% decrease on average per year in CMRgl in all ROIs, while 87 of the 116 AD ROIs had an overall annual *increase* in CMRgl. These non-trimmed results were viewed with skepticism considering they included visits with annualized percent changes greater than 200% across the entire brain. As the trim threshold was increased to 10%, baseline values converged asymptotically to those shown in Fig. 1. All values trimmed in this manuscript were extreme outliers of annualized percent change greater than 100% across the brain between visits. For trim thresholds above the ten percent used in this study, the baseline AD values slowly increase. The trimmed values in this case were directionally biased in the negative direction, likely due to true disease effects. The final trim factor of 10% was selected based on the ability to remove extreme outlying values while retaining meaningful disease effects.

When determining the extent of longitudinal percent signal change, it is necessary to have greater temporal variability than visit variability.
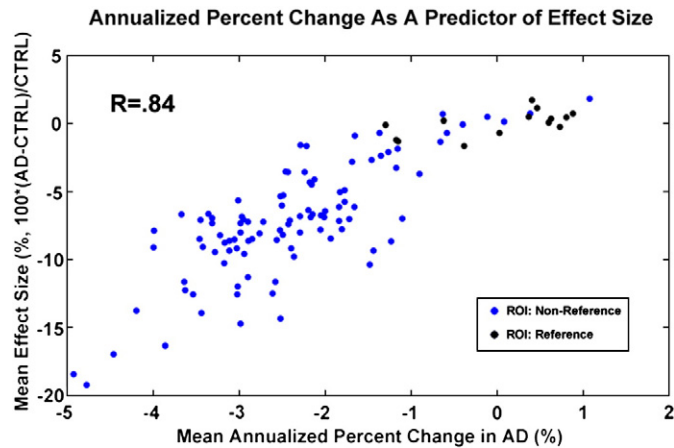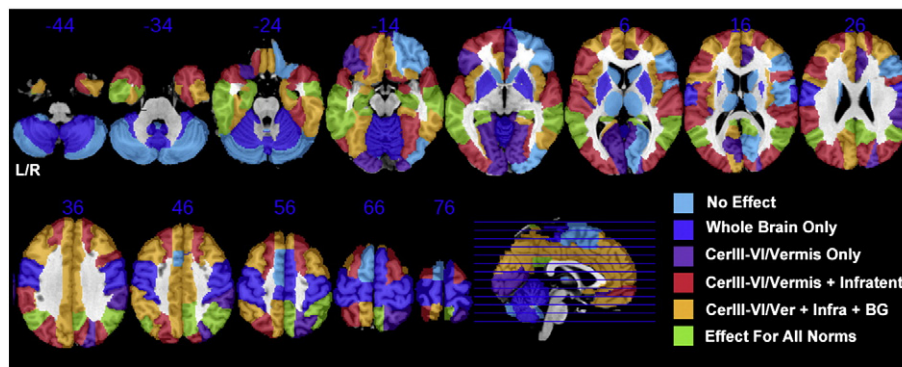
Fig. 6. AAL atlas regions showing significantly lower FDG ratios in Alzheimer's disease patients compared with healthy elderly volunteers by denominator region. Colors reflect significant differences for a given reference region. As an example, ROIs shown to be significant whether using the subset of cerebellum (AAL cerebellum III–VI and vermis) or the entire infratentorial space as a reference region are shown in red. Images shown are in neurological orientation, with the MNI axial coordinate shown in blue.

Because of this, effect sizes between contrasts need to be large. Despite the large variability present in the longitudinal data, two significant trends from the analysis were clear: 1) cerebrum CMRgl decrease over time was greater in AD than in NC and 2) cerebrum CMRgl decrease over time was greater than superior cerebellum CMRgl decrease over time, implying that the superior cerebellum is relatively stable. In addition, rates of change in typically disease-preferred areas are in conformance with previously published findings. These findings demonstrate the heterogeneity present in the dynamics of the disease progression. Not only is this limited to the cerebrum, but to inferior portions of the cerebellum as well, a region classically thought to be relatively spared by the disease. It is precisely this heterogeneity that makes whole brain normalization biased and suggests superior cerebellum as being the more sensitive reference for quantifying disease dynamics in a longitudinal analysis.

Finding the ideal reference region has been cast here as a data-driven problem. COV is a measure of relative stability over time; a small COV suggests little relative change over time, while a large COV points to dynamic behavior. Using a brute force method allows immediate insight into the problem by visual inspection of a single heat map. Initially, based on the longitudinal analysis, one may assume the cerebellum to have the smallest COV, however this is not the case. Recall that these are the ratios of one ROI to another; therefore a small COV often indicates that there is a collinear relationship between two ROIs. Adversely, a large COV indicates that one ROI is changing relative to another, an ideal condition for normalization. As an example of known collinearity, one can look at the square features centered on the matrix diagonal. These are regions that are correlated with tissue very close in space and function to itself. Further visual examination of the features in the group contrast COV map yields immediate insight into the effectiveness of both individual and grouped ROIs. For example, in line with the longitudinal analysis there is a clear difference in using inferior versus superior regions of the cerebellum as a normalizing region, demonstrated by higher intensities horizontally in superior versus inferior cerebellum.

It should be emphasized however, that COV is not a change in overall decreased activity, but the rate of change of activity. Because the numerator of COV is standard deviation, this can be increased noise just as easily as it can be a linear or nonlinear decrease. Noise sources can be attributed to, among other things, mis-registration. Additionally, the denominator of the COV is mean CMRgl across time, which one can argue is smaller in AD patients, particularly in the late stages of the disease. However, this does not discount the metric since the phenotype used in further analysis will benefit from the same scaling bias. Finally, the quantitative analysis of the COV heat maps was largely limited in scope to simple statistics while more sophisticated pattern recognition and clustering methods may yield additional important observations.

In order to validate the assumptions made by qualitative visual inspection of the COV heat maps and inherently noisy non-normalized longitudinal data we chose to evaluate two ROIs using four reference regions identified as candidates for sensitive normalization. The two ROIs chosen, bilateral posterior cingulate and basal ganglia without the caudate, reflected what we believed to be strong decline due to disease and relative sparing respectively. Looking only at posterior cingulate, we demonstrated further motivation for using only the superior portion of the cerebellum. Not only did it prove more significant than all of the other three candidate reference regions in identifying disease related changes, it did so earlier, significantly identifying AD from HC after only a six month time span. Looking at the normalization effects on basal ganglia corroborated the pitfalls of using whole brain normalization in Alzheimer's disease as reported by Borghammer and colleagues [16,17]. The authors found basal ganglia whole-brain ratios in Alzheimer's disease patients appear to increase with age, which is most likely due to larger decreases in whole brain FDG uptake over time compared with decreases in basal ganglia FDG uptake over time.

To focus on the COV methodology the principal findings of this study were limited to the groups with the clearest diagnosis: healthy controls versus probable AD. However, the ADNI sample contains a group of potential early onset subjects labeled as Mildly Cognitive Impaired (MCI). Over the course of the study, subjects that are later diagnosed as AD are considered converters, those that are not, are labeled as non-converters. While the interpretation and findings using the COV method on this sample are thought to be beyond the focus of this manuscript, a brief summary of the results can be found in the supplementary material found accompanying this manuscript, demonstrating degenerative traits found in the MCI group midway between HC and AD. The figures found in this material support the use of COV as a metric for identifying relative dynamic differences among groups and demonstrate the dynamics found within the MCI sub-sample for posterior cingulate, occipital lobe and superior cerebellum ROIs.

The ADNI study is unique in that it provides a large longitudinal sample with which to make inference on the dynamics of the disease. With absolute longitudinal analysis, COV techniques, and normalized longitudinal analysis, we have shown the superior cerebellum to consistently be more sensitive in identifying dynamic changes brought on by the disease than all other AAL ROIs. While dynamic changes are important in understanding the disease, most clinical visits are inherently cross-sectional. Because of this, linking longitudinal changes in each ROI to cross-sectional effects already present at the time of appointment is crucial. We demonstrated strong correlations between the mean cross-sectional effect size and longitudinal percent change. This can be interpreted as, at least in the mild AD stage of the disease, no ROI having detectable

saturation in decline. If an ROI were to have declined to the point of saturation before the AD stage of disease it would elicit a large cross-sectional effect size while showing little or no percent change over time.

Demonstrating annualized percent signal change in AD patients as significantly associated with mean group difference is consistent with the fact that Alzheimer's disease is a progressive neurodegenerative disease. In addition it demonstrates that normalization with the superior cerebellum not only provides FDG ratios that show the largest rate of decline with age, but also shows the largest group differences when comparing PET FDG ratios between Alzheimer's disease patients and other groups. The comparison between AD patients and healthy elderly volunteers on all AAL atlas regions using the full GLM confirms this. The pitfalls of normalization with mean whole brain FDG are consistent with recent findings by Langbaum and colleagues [8], Alzheimer's disease patients showed higher bilateral cerebellum, and sensory motor cortex FDG-whole brain ratios when compared with controls. Conversely, the largest group differences are observed when normalizing with the superior cerebellum as bisected by the horizontal fissure. Coupling this finding with demonstrated stability over time and increased sensitivity to dynamic disease effects provides strong evidence for the use of superior cerebellum as a reference region.

The superior cerebellum defined here can be interpreted as the spinocerebellum and associated vermis together with the cerebellum VI superior to the horizontal fissure. Functionally these areas reflect limb positioning and speech articulation. More importantly, these areas are unique in terms of their blood supply. The superior cerebellum receives its blood supply from the superior cerebellar artery (SCA), whereas the areas inferior to the horizontal fissure receive their supply from the anterior inferior (AICA) and posterior inferior cerebral arteries (PICA). The SCA is adjacent to the posterior cerebral artery (PCA) and might in fact have compensatory reactivity to blockage in the PCA which supplies precuneus, posterior and anterior cingulate. These are among the primary areas along the midline cerebral hemispheres affected in AD. The blood flow from the AICA and PICA are far more related to additional vertebral and basilar artery circulation than the SCA and PCA, which are more closely related to additional Circle of Willis circulation. It is possible that the reduced flow in medial cerebrum regions due to cerebral amyloid angiopathy (reduced FDG uptake in medial cerebrum regions) results in a compensatory increase in blood flow to the superior cerebellum with a corresponding relative increase in FDG uptake in the superior cerebellum region.

We are aware that many recent studies have used the pons as a reference area, this study was limited to regions that currently have a standard definition in the AAL atlas. Atlas based delineations of ROIs have considerable advantages in standardization and analyses of large data sets. Future work on reference region selection should consider using standard atlases that do include the pons or independently generate a pons reference region based on the template, despite the systematic error this may incur between studies. In addition, the relatively small size and scarcity of gray matter in the pons makes it susceptible to increased variability. Another technique commonly used is to restrict the regions to gray matter tissue. While we feel that the hypothesis behind this technique is strong, the standard filter of 8 mm isotropic used by ADNI largely obfuscates gray and white matter introducing partial voluming effects and increases the necessity of accurate registrations to the template, potentially creating a group bias.

5. Conclusions

This work has systematically isolated the superior portion of the cerebellum, including vermis, as being the most sensitive normalizing region for detecting both rates of decline and baseline deficits in Alzheimer's disease. The compiled evidence includes: 1) superior cerebellum was demonstrated to be stable over time in AD patients while the majority of the cerebrum is in decline (including the inferior cerebellum), 2) COV analysis isolated the basal ganglia along with the cerebellum (particularly superior cerebellum) as being the most sensitive normalizing region over time, 3) grouping ROIs, superior cerebellum detected group differences 6 months before full cerebellum and 18 months before whole brain and basal ganglia normalization, 4) rates of decline were significantly correlated with and therefore indicative of already present disease effects when using the superior cerebellum, and 5) the extent and magnitude of baseline differences between AD and HC were greatest when normalizing by superior cerebellum.

Appendix A. Supplementary data

Supplementary data to this article can be found online at doi:10.1016/j.bbadis.2011.09.008.

References

[1] S. Minoshima, K.A. Frey, N.L. Foster, D.E. Kuhl, Preserved pontine glucose metabolism in Alzheimer disease: a reference region for functional brain image (PET) analysis, J. Comput. Assist. Tomogr. 19 (1995) 541–547.
[2] J.L. Andersson, How to estimate global activity independent of changes in local activity, Neuroimage 6 (1997) 237–244.
[3] I. Yakushev, A. Hammers, A. Fellgiebel, I. Schmidtmann, A. Scheurich, H.G. Buchholz, J. Peters, P. Bartenstein, K. Lieb, M. Schreckenberger, SPM-based count normalization provides excellent discrimination of mild Alzheimer's disease and amnestic mild cognitive impairment from healthy aging, Neuroimage 44 (2009) 43–50.

[4] P. Borghammer, J. Aanerud, A. Gjedde, Data-driven intensity normalization of PET group comparison studies is superior to global mean normalization, Neuroimage 46 (2009) 981–988.

[5] P.T. Fox, M.A. Mintun, E.M. Reiman, M.E. Raichle, Enhanced detection of focal brain responses using intersubject averaging and change-distribution analysis of subtracted PET images, J. Cereb. Blood Flow Metab. 8 (1988) 642–653.

[6] M. Kushner, M. Tobin, A. Alavi, J. Chawluk, M. Rosen, F. Fazekas, J. Alavi, M. Reivich, Cerebellar glucose consumption in normal and pathologic states using fluorine-FDG and PET, J. Nucl. Med. 28 (1987) 1667–1670.

[7] R. Mielke, U. Pietrzyk, A. Jacobs, G.R. Fink, A. Ichimiya, J. Kessler, K. Herholz, W.D. Heiss, HMPAO SPET and FDG PET in Alzheimer's disease and vascular dementia: comparison of perfusion and metabolic pattern, Eur. J. Nucl. Med. 21 (1994) 1052–1060.

[8] J.B. Langbaum, K. Chen, W. Lee, C. Reschke, D. Bandy, A.S. Fleisher, G.E. Alexander, N.L. Foster, M.W. Weiner, R.A. Koeppe, W.J. Jagust, E.M. Reiman, Categorical and correlational analyses of baseline fluorodeoxyglucose positron emission tomography images from the Alzheimer's Disease Neuroimaging Initiative (ADNI), Neuroimage 45 (2009) 1107–1116.

[9] W.S. Liang, K. Chen, W. Lee, K. Sidhar, J.J. Corneveaux, A.N. Allen, A. Myers, S. Villa, B. Meechoovet, J. Pruzin, D. Bandy, M.J. Huentelman, K. Jensen, T. Dunckley, R.J. Caselli, S. Kaib, E.M. Reiman, Association between GAB2 haplotype and higher glucose metabolism in Alzheimer's disease-affected brain regions in cognitively normal APOEepsilon4 carriers, Neuroimage 54 (2010) 1896–1902.

[10] A. Loessner, A. Alavi, K.U. Lewandrowski, D. Mozley, E. Souder, R.E. Gur, Regional cerebral function determined by FDG-PET in healthy volunteers: normal patterns and changes with age, J. Nucl. Med. 36 (1995) 1141–1149.

[11] C. Messa, D. Perani, G. Lucignani, A. Zenorini, F. Zito, G. Rizzo, F. Grassi, A. Del Sole, M. Franceschi, M.C. Gilardi, et al., High-resolution technetium-99m-HMPAO SPECT in patients with probable Alzheimer's disease: comparison with fluorine-18-FDG PET, J. Nucl. Med. 35 (1994) 210–216.

[12] K. Kantarci, M.L. Senjem, V.J. Lowe, H.J. Wiste, S.D. Weigand, B.J. Kemp, A.R. Frank, M.M. Shiung, B.F. Boeve, D.S. Knopman, R.C. Petersen, C.R. Jack Jr., Effects of age on the glucose metabolic changes in mild cognitive impairment, AJNR Am. J. Neuroradiol. 31 (2010) 1247–1253.

[13] K.B. Walhovd, A.M. Fjell, J. Brewer, L.K. McEvoy, C. Fennema-Notestine, D.J. Hagler Jr., R.G. Jennings, D. Karow, A.M. Dale, Combining MR imaging, positron-emission tomography, and CSF biomarkers in the diagnosis and prognosis of Alzheimer disease, AJNR Am. J. Neuroradiol. 31 (2011) 347–354.

[14] K.B. Walhovd, A.M. Fjell, A.M. Dale, L.K. McEvoy, J. Brewer, D.S. Karow, D.P. Salmon, C. Fennema-Notestine, Multi-modal imaging predicts memory performance in normal aging and cognitive decline, Neurobiol. Aging 31 (2011) 1107–1121.

[15] S.M. Landau, D. Harvey, C.M. Madison, R.A. Koeppe, E.M. Reiman, N.L. Foster, M.W. Weiner, W.J. Jagust, Associations between cognitive, functional, and FDG-PET measures of decline in AD and MCI, Neurobiol. Aging (2009).

[16] P. Borghammer, K.Y. Jonsdottir, P. Cumming, K. Ostergaard, K. Vang, M. Ashkanian, M. Vafaee, P. Iversen, A. Gjedde, Normalization in PET group comparison studies—the importance of a valid reference region, Neuroimage 40 (2008) 529–540.

[17] P. Borghammer, P. Cumming, J. Aanerud, A. Gjedde, Artefactual subcortical hyperperfusion in PET studies normalized to global mean: lessons from Parkinson's disease, Neuroimage 45 (2009) 249–257.

[18] S.G. Mueller, M.W. Weiner, L.J. Thal, R.C. Peterson, J. Clifford, W.J. Jagust, J.Q. Trojanowski, A.W. Toga, L. Becket, Alzheimer's Disease Neuroimaging Initiative, in: A. Fisher, M. Memo, F. Stocchi, I. Hanin (Eds.), Advances in Alzheimer's and Parkinson's Disease: Insight Progress and Perspectives, vol. 57, Springer, 2008, pp. 183–197.

[19] M.F. Folstein, S.E. Folstein, P.R. McHugh, "Mini-mental state". A practical method for grading the cognitive state of patients for the clinician, J. Psychiatr. Res. 12 (1975) 189–198.

[20] L. Berg, Clinical dementia rating (CDR), Psychopharmacol. Bull. 24 (1988) 637–639.

[21] W.G. Rosen, R.C. Mohs, K.L. Davis, A new rating scale for Alzheimer's disease, Am. J. Psychiatry 141 (1984) 1356–1364.

[22] G. McKhann, D. Drachman, M. Folstein, R. Katzman, D. Price, E.M. Stadlan, Clinical diagnosis of Alzheimer's disease: report of the NINCDS-ADRDA work group under the auspices of Department of Health and Human Services Task Force on Alzheimer's Disease, Neurology 34 (1984) 939–944.

[23] F. Kruggel, D. Yves von Cramon, Alignment of magnetic-resonance brain datasets with the stereotactical coordinate system, Med. Image Anal. 3 (1999) 175–185.

[24] S. Hentschel, F. Kruggel, Determination of the intracranial volume: a registration approach, in: T. Jiang (Ed.), International Workshop on Medical Imaging and Augmented Reality (MIAR 2004), Lecture Notes in Computer Science, vol. 3150, Springer, Berlin, 2004, pp. 253–260.

[25] G. Wollny, F. Kruggel, Computational cost of nonrigid registration algorithms based on fluid dynamics, IEEE Trans. Med. Imaging 21 (2002) 946–952.

[26] N. Tzourio-Mazoyer, B. Landeau, D. Papathanassiou, F. Crivello, O. Etard, N. Delcroix, B. Mazoyer, M. Joliot, Automated anatomical labeling of activations in SPM using a macroscopic anatomical parcellation of the MNI MRI single-subject brain, Neuroimage 15 (2002) 273–289.

[27] M. Bentourkia, A. Bol, A. Ivanoiu, D. Labar, M. Sibomana, A. Coppens, C. Michel, G. Cosnard, A. De Volder, Comparison of regional cerebral blood flow and glucose metabolism in the normal brain: effect of aging, J. Neurol. Sci. 181 (2000) 19–28.

[28] L.M. Parkes, W. Rashid, D.T. Chard, P.S. Tofts, Normal cerebral perfusion measurements using arterial spin labeling: reproducibility, stability, and age and gender effects, Magn. Reson. Med. 51 (2004) 736–743.

[29] Y. Chen, D.J. Wang, J.A. Detre, Test–retest reliability of arterial spin labeling with common labeling strategies, J. Magn. Reson. Imaging 33 (2011) 940–949.